Miettinen, Mikael; Vainio, Valtteri; Theska, René; Viitala, Raine

Aerostatically sealed chamber as a robust aerostatic bearing

Published in:
Tribology International

DOI:
10.1016/j.triboint.2022.107614

Published: 01/09/2022

Document Version
Publisher's PDF, also known as Version of record

Please cite the original version:
Miettinen, M., Vainio, V., Theska, R., & Viitala, R. (2022). Aerostatically sealed chamber as a robust aerostatic bearing. *Tribology International*, *173*, Article 107614. https://doi.org/10.1016/j.triboint.2022.107614

Tribology International 173 (2022) 107614

Contents lists available at ScienceDirect

Tribology International

journal homepage: www.elsevier.com/locate/triboint

Aerostatically sealed chamber as a robust aerostatic bearing

Mikael Miettinen [a,*], Valtteri Vainio [a], René Theska [b], Raine Viitala [a]

[a] *Department of Mechanical Engineering, Aalto University, Espoo, Finland*
[b] *Precision Engineering Group, TU Ilmenau, Germany*

ARTICLE INFO

Keywords:
Aerostatic Bearing
Porous restrictor
Deflection compensation
Robust design

ABSTRACT

Aerostatic bearings are typically used in ultra precision and high speed applications in controlled environments. The present study expands this operating domain. The present study experimentally investigates the performance and feasibility of a novel design for a robust air bearing consisting of an aerostatically sealed pressurized volume. A suitable operating domain for the bearing system was characterized based on measurements of the load capacity, friction moment, chamber flow, and seal flow rate at various opposing surface run-outs and supply pressures. The highest measured load capacity was 18.86 kN at 0.330 mm run-out, and decreased to 12.22 kN load at 3.804 mm run-out. The study provided corroborative evidence on the feasibility of the proposed chamber based bearing design.

1. Introduction

Gas-lubricated bearings are common in precision motion and positioning, for example, in high-speed rotating machines and precision measuring and machining tools. Typically, air is used as the lubricant in the bearings, due to its appropriateness, availability and low cost due to existing air supply networks. Using gas as the lubricant results in low friction and small gap height due to the low viscosity of gasses. In order to maintain the proper gap height, usually in the range of 2–20 μm, narrow manufacturing tolerances for the system components are required. For the typical applications, the main benefit of air bearings has been the improved positioning accuracy and low friction at high speeds.

However, as the world is transitioning towards a more sustainable future, the energy efficiency of industrial processes has to be reconsidered. For example, the European Green Deal aims to reduce the greenhouse gas emissions by 50% from the emission level of 1990 before the year 2030 [1]. In order to meet this goal in the paper and cardboard industry, losses in the production process should be minimized. Currently, 15–25% of the total energy consumed in paper machines is used to overcome friction [2].

The bearings used in the rolls of these machines are commonly rolling element, hydrostatic or hydrodynamic bearings. In particular, the energy consumption of the hydrodynamic bearing system in deflection-compensated rolls is enormous [3]. The energy consumption consists of the pumping and cooling of the fluid in addition to the power to overcome the high rotational friction of the roll due to the high viscosity of the fluid. The bearing system of deflection compensated rolls consist of end bearings that locate the shell in relation to the shaft and deflection compensation bearings that span the whole length of the roll. The deflection-compensated rolls have an internal mechanism to counteract the external load acting on the shell of the roll, minimizing the deflection of the shell and thus improving end product, such as paper or carboard quality (Fig. 1.). In particular, the improved quality is seen as a more even thickness and gloss along the product cross direction, i.e., the roll axis direction. Replacing the energy intensive hydrostatic and dynamic bearings in deflection-compensated rolls by aerostatic bearings could significantly reduce the total energy consumption of the roll systems that consists of drive, pumping and cooling power.

Aerostatic bearings have been extensively researched in various applications, which are showcased in a recent review article by Gao et al. [4]. Porous and orifice-compensated aerostatic bearings have been studied extensively by, for example, in a comparison between orifice, porous and partially porous bearings by Fourka and Bonis [5]. Due to the rise of additive manufacturing, novel design for orifice geometry have emerged [6]. There has been research on increasing the stiffness of aerostatic bearings, such as regulator valve by Ghodsiyeh et al. [7]. Additionally, actively compensated aerostatic bearings, where the inlet orifices were adjusted by piezoelectric actuators and voice coils, have been investigated by Theisen et al. [8,9], Morosi and Santos [10] and Maamari et al. [11].

Porous restrictor bearings are a subset of the aerostatic bearings. The

* Corresponding author.
E-mail address: mikael.miettinen@aalto.fi (M. Miettinen).

https://doi.org/10.1016/j.triboint.2022.107614
Received 7 March 2022; Received in revised form 20 April 2022; Accepted 29 April 2022
Available online 4 May 2022

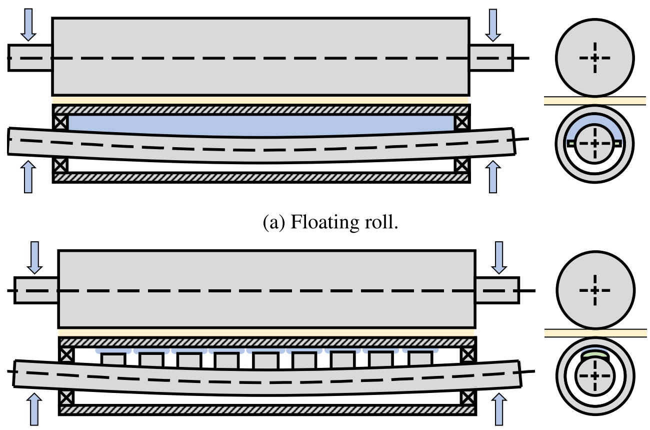

(a) Floating roll.

(b) Zone compensated roll.

Fig. 1. Deflection-compensated rolls, where a rotating roll shell is supported by a stationary shaft. External loading is counterbalanced with loading from an internal deflection compensation mechanism. Figure not-to-scale.

main advantages of porous aerostatic bearings are the good load carrying properties and the robustness against scratches and defects due to the even distribution of air into the air gap [12]. Additionally, the porous bearings rarely have self-induced vibrations, that are commonly referred as *pneumatic hammer* instability. Numerical models of the bearings have been developed, for example, a resistor network model of a journal bearing with surface restrictive layer by Otsu et al. [13] and an 1D model of flat circular bearing pads by Plante et al. [14]. Additionally, a comparison of 1D and 3D models for porous bearings including a validation with experimental data is presented by Luong et al. [15].

In addition to using aerostatic elements as bearings, the elements can be used as seals. Aerostatic seals are a type of non-contact seals, that use an externally pressurized region in a narrow gap to limit flow from one side to the other. Aerostatic seals have been researched mainly in the context of turbomachinery and vacuum applications. Additionally, there are designs that combine both bearing and sealing functions into the same aerostatic element. Depending on the design of the aerostatic element, it can be used as either a seal or a bearing, or used as both a seal and a bearing at the same time.

Aerostatic seals can have at least two modes of operation (Fig. 2). In the first mode (a), the pressure in the seal gap is higher than in the high pressure side of the seal. Thus, the seal supply gas flows through the restrictor and the seal gap into both the high pressure and the low pressure side of the seal. In the second mode, the pressure in the seal gap is lower than the pressure on the high pressure side of the seal. Thus, the gas from the high pressure side leaks through the seal gap into the low pressure side. However, the flow is restricted by the seal gap. In between these modes, there is a point where the pressure on the high pressure side of the seal is equal to the pressure in the seal gap. At this point, there is virtually no flow to or from the high pressure side, excluding flows due to external disturbances such as the relative motion of the seal and its opposing surface, and the seal supply flows to the low pressure side.

The sealing mode depends on the pressure in the seal gap. The seal gap pressure depends on the seal supply pressure, the seal restriction, and the restriction of the seal gap. The seal gap height affects the restriction on the gas flow through the seal, including both leakage from the chamber and the seal flow. Therefore, determining the actual pressure in the seal gap is not trivial. However, the effects of the seal gap pressure can be observed from the flow behavior of the seal.

One of the studied types of aerostatic seal is an externally pressurized labyrinth. Messenger et al. [16,17] have developed and experimentally validated such aerostatic sealing system for turbomachinery. The seal in Messenger's studies was pressurized from the high pressure side of the seal and was preloaded to not contact the shaft at low pressures. Zimmermann et al. [18,19] have developed a test setup for investigating adaptive seals, which are combinations of labyrinth and orifice-compensated aerostatic seals. The adaptive seals are further studied by Wilhelm et al. [20].

Seals using porous graphite restrictors have also been studied. Devitt and Kirkpatrick [21] developed a vacuum chamber using an aerostatic element simultaneously as a seal for the vacuum and as a guide for a linear stage. Additionally, Khim and Park [22] used porous seals and bearings to construct a rotary table penetrating inside a vacuum chamber and Heidler [23] investigated the use of gas bushing in vacuum conditions as guides.

Despite this prior research considering for example a vacuum chamber sealing [21], the current body of knowledge lacks published research on air-bearing-sealed pressure chambers for force generation virtually without contact to the opposing surface. The force-transmitting medium is the pressurized gas. The virtually contactless operation with a low viscosity fluid as a transmitting fluid enables the usage against fast moving opposing surfaces found for example in rotor systems. The relatively low load carrying capacity of aerostatic systems can be compensated with increased bearing area.

A promising utilization for such force producing aerostatically sealed pressure chamber would be a bearing solution for large flexible rotors, such as paper and cardboard machine rolls. The rolls are flexible rotors, and typically have large length to diameter ratio [24]. The large size, weight and flexibility of the rolls, in addition to the continuous manufacturing process where the rolls are operated, poses requirements for the robustness, and misalignment and surface planarity (or, in rotating machine applications, surface roundness) tolerances of the bearing systems. The current air bearing designs cannot fulfill these requirements without incurring significant additional costs, for example, related to the very narrow tolerances of the air bearing opposing surface (in the order of half the gap height).

The following research questions were addressed in the present study: .

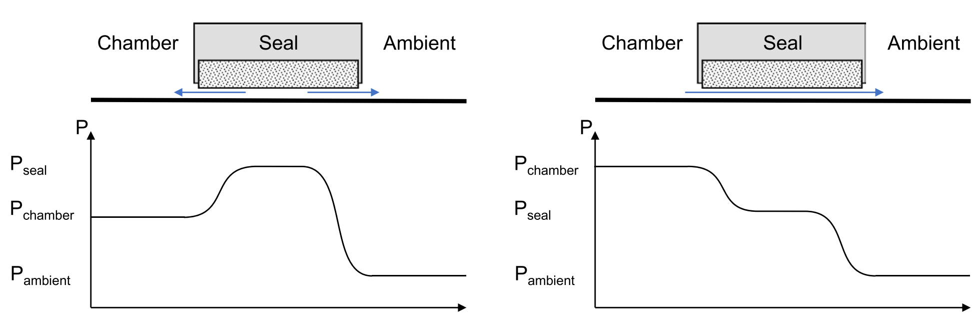

(a) Seal flow mode.

(b) Chamber leakage mode.

Fig. 2. Sealing modes. An aerostatic seal can operate in either mode depending on the pressure level in the seal gap, chamber (high pressure) and ambient (low pressure).

1. What is the suitable operating parameter range of a chamber based aerostatic bearing? Which factors limit the suitable operating range?
2. How does the run-out of the opposing surface affect the performance of a chamber based aerostatic bearing?

Thus, in the present study we report a contribution beyond the state-of-the-art: .

1. A novel method and design to construct a robust aerostatic bearing for large load applications.
2. A novel flexibly supported aerostatic seal design and method to seal a pressure chamber against a moving opposing surface without requirements for narrow manufacturing tolerances.
3. A realized design of the previous two and an experimental performance measurement setup.
4. A thorough test data set with analysis investigating the performance of such a system in various conditions regarding pressure levels, loads, friction and run-out of the opposing surface.

These contributions resulted in the following new findings: .

1. The limiting factor to the suitable operating range is the seal gap height; too low and the seal contacts the opposing surface, too high and the seal leaks.
2. Increased run-out decreases the load capacity of the bearing.
3. The design for the robust aerostatic bearing is feasible, considering the load capacity and air consumption.

2. Methods

2.1. Bearing design

The investigated bearing unit consists of an aerostatic seal that seals a volume between the bearing frame and the opposing surface. The bearing and its parts are shown in Fig. 3. The sealed volume of the bearing was pressurized in order to increase the load capacity of the bearing. A floating seal design was used, where the seal body was mounted with flexures that allowed displacement and tilting. The seal was preloaded against the opposing surface in order to maintain the desired air gap height between the seal and the opposing surface. The pressurized volume was the main load carrying element of the system and the load capacity of the seal was used to offset the preload acting on the seal.

Porous graphite restrictor was used in the seal and the graphite was attached to the relatively flexible aluminium body with epoxy [25,26]. The width of the graphite seal face was 15 mm, and the thickness of the graphite was 4.5 mm. The distribution groove in the seal body was 7 mm wide and 2 mm deep. The groove distributes the pressurized air evenly to the backside of the porous material. The dimensions of the seal and related features are presented in Fig. 4. The dimensions of the chamber, i.e., the internal dimensions of the seal were 270 mm in the horizontal direction and 120 mm in the vertical direction, with a 60 mm radius arcs at both ends. The area of the seal face was 0.011 m^2 and the area and the volume of the pressurized volume were 0.029 m^2 and 0.203 L, respectively.

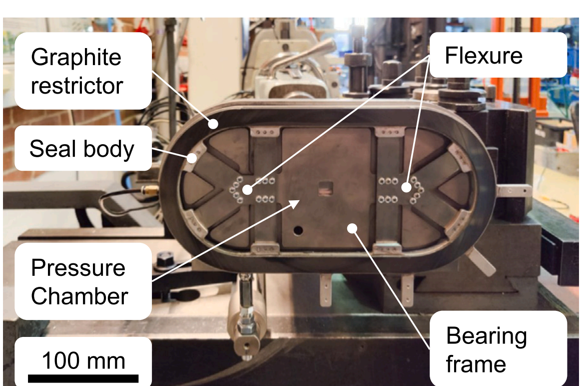

Fig. 3. The investigated bearing consisting of an aerostatically sealed pressure chamber. The seal is mounted with flexures to the bearing frame; thus it can float freely.

The seal body was flexibly mounted to the bearing frame with flexures made of 0.5 mm thick stainless steel sheet. The flexures allow a range of motion of ± 2 mm, corresponding to angular motion of ± 1.64° in the vertical direction and ± 0.85° in the horizontal direction. The main limiting factor of the seal displacement was the clearance between the seal body and the bearing frame. The difference in angular motion range in vertical and horizontal direction is due to the dimensions of the pressure chamber. The floating design allows the seal to maintain a constant air gap height, allows greater misalignment and displacement between the seal and the opposing surface during operation, and compensates for the manufacturing inaccuracies of the components. The seal was preloaded against the opposing surface by a pressurized loop of silicone tube located in a groove of the bearing frame. The combined stiffness of the preload tube and the flexures should be lower than the stiffness of the air film in the air gap, in order to have the seal follow the opposing surface as desired. The silicone tube had a 12 mm internal diameter and a 15.5 mm external diameter and the groove that located the tube was 9 mm deep and 17 mm wide. The width of the groove was selected so that the internal width of the tube matches the width of the seal face. Additionally, the tube was glued in place with moisture curing silicone adhesive in order to form a pressure-tight seal between the silicone tube, the seal body and the bearing frame.

The permeability of the porous material is determined from the short circuit flow of the bearing. The permeability of porous material [25] is defined as

$$\kappa = \frac{2\,Q\,\mu\,h\,p_a}{A\,(p_s{}^2 - p_a{}^2)}, \tag{1}$$

where Q is the measured short circuit flow rate, η is the dynamic viscosity, h is the thickness of the porous material, A is the area of the seal face, P_s is the supply pressure and P_a is the ambient pressure.

2.2. Test setup

The test setup consisted of the bearing described in the previous section, the pneumatic system to supply the pressurized air, and sensors and data acquisition equipment to measure the occurring phenomena. There are many types of test setups for aerostatic bearings found in the literature, that have similarities and differences to the investigates setup. The load on the bearing is commonly generated by weights or an actuator such as a screw or a pneumatic cylinder [12,27]. Commonly the bearings are tested against a static surface. However, in the present setup the load was generated by the sealed pressure chamber itself, as the flexure mounted seals allow for displacement of the system under load and the opposing surface was rotating.

The test setup was built on a TOS SN 63 C lathe, as is shown in Fig. 5.

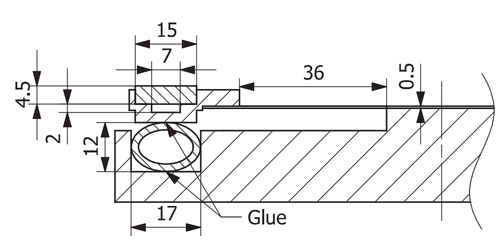

Fig. 4. A cross-section of the seal with dimensions. The preload tube is glued to the back of the seal body and the bottom of the groove of the bearing frame.

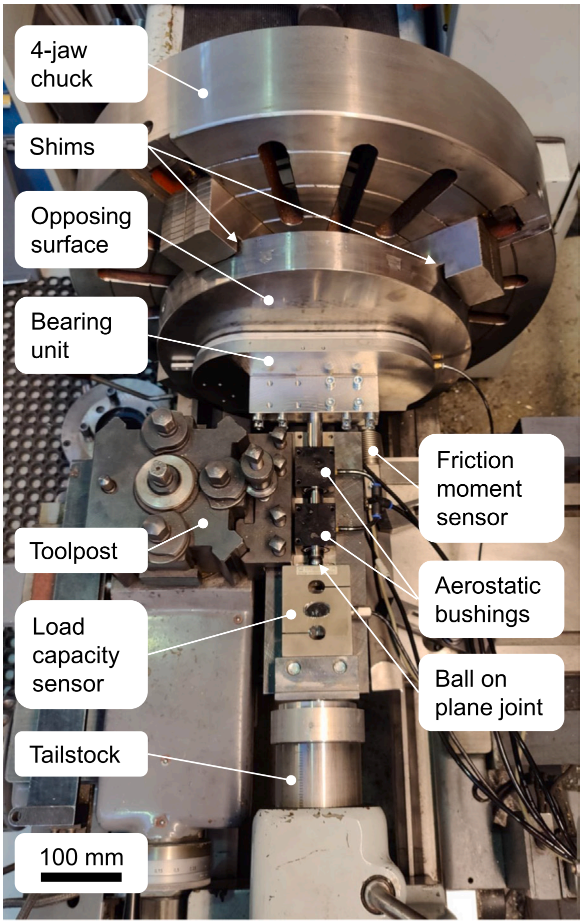

Fig. 5. The test setup on the lathe.

A detailed drawing of the bearing is additionally shown in Fig. 6. The bearing unit was mounted on the toolpost of the lathe. Additionally, the bearing unit was supported by the tailstock in the axial direction in order to carry the high axial load. The support from the tailstock was required in order to not overload the compound slide of the lathe. The axial load of the bearing is supported with the tailstock of the lathe, through a force transducer that is used to measure the actual load capacity of the developed system. Additionally, the rotational degree of freedom of the bearing was designed to be as frictionless as possible: the bearing is supported with aerostatic bushings in the radial direction and the axial support is through a ball on plane contact. A hardened steel ball, that was mounted on the end of the shaft of the bearing, acted against the flat end of a carbide pin on the force transducer. This ensured that the contact between the aerostatic seal and the opposing surface was accurately detected, when the system reached its performance limits.

The opposing surface of the bearing was a 400 mm diameter steel disk with a thickness of 40 mm. In the investigated load range, no significant deformation of the disk is expected. The surface roughness of the steel disk was 0.16 Ra. The disk was held in the independently adjustable four-jaw chuck of the lathe. The axial run-out, i.e., the wobble of the steel disk was varied by placing steel shims between the disk and two neighboring jaws of the chuck. The axial alignment was varied to investigate the resistance of the bearing system to misalignment and vibration of the system. The shims were used to support the axial load of the bearing acting on the disk, thus negating the possibility of the disk moving in the chuck during the measurements. The amount of wobble of the steel disk was measured by the axial run-out, as is defined in ISO1101:2017 [28]. The axial run-out was measured at a 190 mm radius from the axis of rotation with a digital indicator. See the different Axial run-outs used in the experiments in Table 2.

2.2.1. *Pneumatic system*

The test setup included a pneumatic system that allowed the control and measurement of the pressures and flow rates in each part of the seal and pressure chamber system. Three pressures were individually controlled with the pressure regulators: seal pressure, preload pressure, and chamber pressure. The measured flow rates were the seal supply flow and the chamber flow, individual sensors were used for flow in and out of the chamber as the sensors used were unidirectional. The flow in the chamber supply can be to either direction depending on the pressure level in the seal gap and the chamber (Fig. 2). The regulators were controlled with analogue signals generated by the data acquisition device. A diagram of the pneumatic system is presented in Fig. 7 and the specifications of the sensors and pressure regulators used are presented in Table 1.

2.2.2. *Calibration*

The force and moment sensors were calibrated. The calibration was performed at three points, 0–5–10 Nm for the friction moment force transducer and 0–5–10 kN for the load capacity force transducer. A linear curve was fitted to the results and the curve values were used to set the *zero* and *gain* values for the sensors in the data acquisition

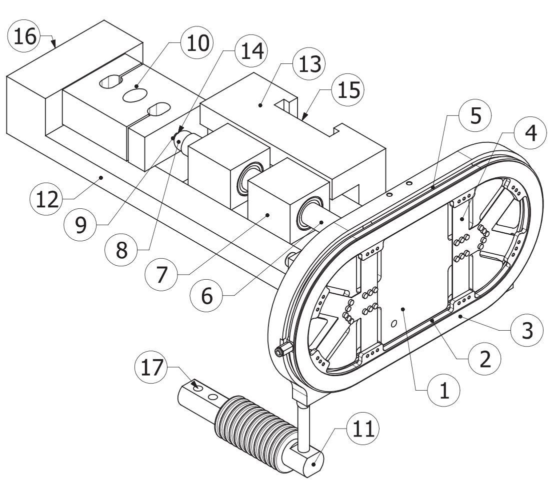

Identifier	Name / Explanation	Quantity
1	Bearing frame	1
2	Seal body	1
3	Graphite restrictor	1
4	Flexure	2
5	Preload tube	1
6	Shaft	1
7	Air bushing	2
8	Steel bearing ball	1
9	Carbide pin	1
10	Load force transducer	1
11	Moment force transducer	1
12	Bottom plate	1
13	Toolholder	1
14	Ball on plane contact	1
15	Attached to the toolpost	1
16	Supported by the tailstock	1
17	Attached to the lathe carriage	1

Fig. 6. Drawing of the investigated aerostatically sealed chamber bearing with its mounting parts. The bearing was mounted on a shaft, that was radially supported by aerostatic bearings and axially by a ball on plane contact, thus the friction moment and the load capacity could be measured. In addition to the parts (Identifiers 1–13), attachments and supports to the lathe are shown (Identifiers 14–17).

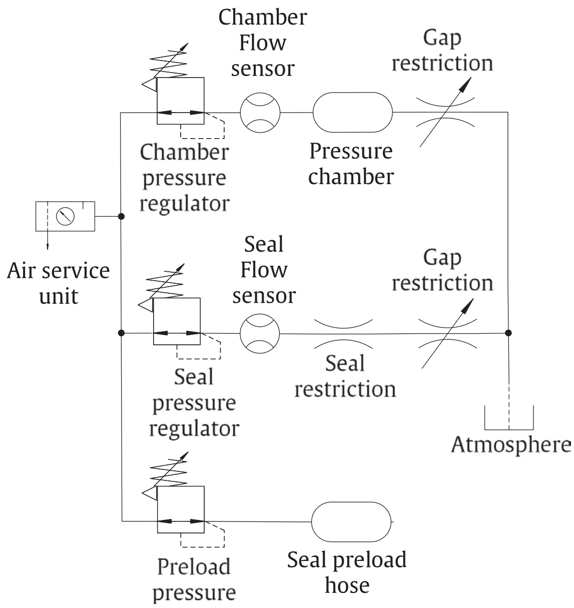

Fig. 7. The pneumatic system of the test setup. Pressure regulators were controlled by analogue voltage signals. The gap restriction varies depending on the gap height and affects seal supply flow and chamber leakage in different amounts due to differences in flow path lengths.

Table 1
Sensors used in the measurement setup.

Device	Type	Range	Accuracy
Seal pressure regulator	Festo VPPM-6 L-L-1-G18–0L10H-V1P-S1C1	0–1 MPa	± 1% FS
Chamber pressure regulator	Festo VPPM-6 L-L-1-G18–0L6H-V1P-S1C1	0–0.6 MPa	± 1% FS
Preload pressure regulator	SMC ITV1050–31F1CL3	0–0.6 MPa	± 2% FS
Seal flow sensor	SMC PFM7–50-C6-E	1–50 l/min	± 5% FS
Chamber in flow sensor	SMC PFM7–50-C6-E	1–50 l/min	± 5% FS
Chamber out flow sensor	SMC PFM7–10-C6-E	1–10 l/min	± 5% FS
Load capacity force transducer	HBM S9	50 kN	± 1% FS
Friction moment force transducer	Raute Precision BA3–100 kg-F	981 N	± 1% FS

software.

The force transducer for the friction moment was calibrated in-place by loading the system through a moment wrench attached to the square socket on the bearing frame. The in-place calibration eliminated uncertainties related to the length of the moment arm. However, the force transducer was calibrated by known weights and a lifting tool that loads the transducer in compression. The calibration was done in vertical orientation due to simplifying the setup, as the errors due to the mass of the sensor are small compared to the measured loads.

2.2.3. *Control and data acquisition*

The lathe spindle speed was controlled manually. All the other control as well as data acquisition were realized with National Instruments cDAQ system, consisting of a CDAQ-9174 chassis equipped with measurement modules NI-9220 for analogue signal inputs (read the pressure and flow sensor signals), NI-9219 for force transducer inputs with full-bridge connections, NI-9411 for trigger signal input from the encoder, and NI-9263 for analogue output signal generation to control the pressure regulators. The control and measurement program was implemented in LabVIEW, which finally saved the data into text files.

The measurements used a Heidenhain ROD 420 incremental encoder with 1024 pulses per revolution as the trigger source. The encoder was attached to the spindle of the lathe.

2.3. *Procedure of experiments*

The measurements of the occurring phenomena were conducted with the procedure described in this section. The measured operating points were limited by the maximum possible supply pressure of 0.6 MPa, maximum allowable leakage of 50 l/min from the chamber and maximum allowable friction moment of 4 Nm. The friction moment was chosen to be an elegant way to detect contact between the graphite aerostatic seal and the opposing surface. The selected maximum leakage is the maximum measurable value of the flow rate sensor, and the friction moment limit was selected at a value where the loading unit is already significantly contacting with the opposing surface. At each measured operating point, 10240 points, i.e., 10 revolutions of 1024 samples per revolution were measured. The measurement program in LabVIEW followed the logic described in Fig. 8.

The following procedure was used in the measurements: .

1. The steel disk used as the opposing surface was adjusted to the desired axial run-out.

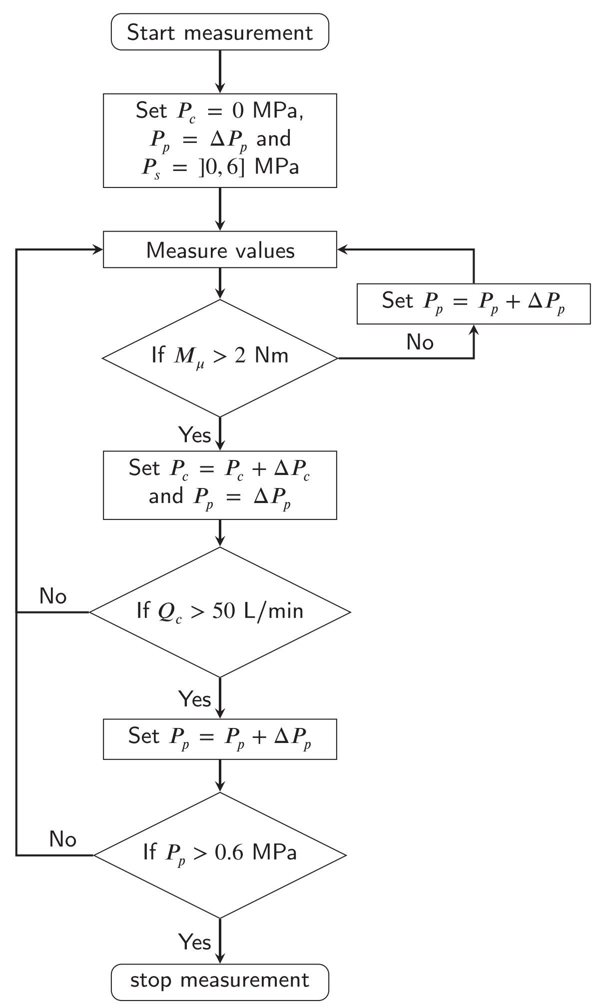

Fig. 8. Flow chart of the logic in the measurement program to map the possible operational parameter combinations. Where P_c is chamber pressure, ΔP_c is chamber pressure step, P_p is preload pressure, ΔP_p is preload pressure step, P_s is seal supply pressure, M_μ is friction moment, and Q_c is chamber flow rate.

2. The lathe carriage was moved until the seal contacted the opposing surface, the tailstock was positioned to carry the axial load and the locking mechanism of the tailstock was tightened.
3. The air supply was turned on and the seal supply pressure was set to 0.6 MPa pressure.
4. The spindle speed of the lathe was set to 260 rpm.
5. The measurement program was started. The program varies the preload and chamber pressures to map out a matrix of suitable operating points. The suitable operating points were determined by the leakage from the chamber and by the friction moment. Values for pressures, flow rates, load capacity, and friction moment were recorded at each measurement point after the values had settled to stable values.
6. After measuring at each suitable operating point, the lathe and the air supply were turned off. The procedure was repeated until the performance under all desired axial run-outs was examined.

2.4. Analysis methods

The measured data consisted of the following:

- 3 pressures: seal pressure, chamber pressure, preload pressure.
- 3 flows: seal flow, chamber flow in and chamber flow out (the flow sensor type used was capable of measuring flow only in one direction).
- 2 loads: load capacity and friction moment.

The data was analysed in Matlab. The following analyses are presented in the study:

- The load capacity, chamber flow and friction moment are presented as a function of the chamber pressure and the preload pressure. The third dimension under investigation is presented utilizing a heatmap. The values for load capacity, chamber flow, seal flow and friction moment are an average of the samples measured at each operating point.
- The useful operating range is limited with yellow and red lines. The lines correspond to constant friction (1 Nm) and no chamber flow (0 l/min), respectively.
- The maximum performance is located at the intersection of the aforementioned lines.
- The theoretical load capacity presented in Table 2 is calculated assuming that the whole area of the bearing, including the chamber and the seal has a uniform pressure distribution equal to the chamber pressure.

3. Results

The permeability of the graphite [25] was 1.06×10^{-15} m^2, calculated from the measured short circuit flow of 20.08 l/min at 0.6 MPa supply pressure.

The load capacity, air consumption and friction measured at various axial run-outs of the opposing surface are presented in Fig. 9. The load capacity graphs show that, intuitively, the load capacity increases with the increasing chamber pressure. As expected, the highest load capacity and operating point with the highest performance was found using the smallest run-out of the rotating opposing surface. The operational range of the bearing was limited by high friction originating from contact with the opposing surface and by high leakage out of the chamber due to insufficient preload to keep the air gap small enough to form a seal.

The chamber flow graphs of the results Fig. 9 shows the two sealing modes presented in Fig. 2. The red contour indicates the preload and chamber pressure combination which results in stagnation of the chamber flow, i.e., chamber flow is 0 l/min, marking the division between the two sealing modes. Furthermore, the chamber pressure is equal to the pressure in the seal gap in order for the chamber flow to stagnate. The negative chamber flow rates indicate sealing mode a), where the seal leaks into the chamber and the pressure regulator exhaust air out in order to maintain the determined chamber pressure level. The positive chamber flow rates indicate sealing mode b), where the chamber leaks to ambient atmosphere and the pressure regulator lets air into the chamber to maintain the determined pressure level. Consequently, the *operational range* of the bearing is limited to the more efficient sealing mode a) where there is no excessive leakage from the chamber, either past the seal or through the regulator exhaust.

The friction moment graphs of the results Fig. 9 show the determination of the friction based limit for the *operational range*. Since the device was almost frictionlessly supported in the rotational degree of freedom (airbushings and hardened steel ball against flat carbide face, see Section 2.2), locking the rotating motion with a moment sensor enabled an elegant manner to recognize the contact between the graphite aerostatic seal and the opposing surface: contact increases the friction between the opposing surface and the bearing. The seal gap height depends on the combination of seal supply pressure (held constant during the measurements), the preload pressure and the chamber pressure. Increasing the preload pressure consequently pushes the seal towards the opposing surface harder and a finally the graphite based aerostatic bearing functioning as a seal cannot sustain the load and a contact is made. Thus, when the preload pressure is high enough in relation to the chamber pressure, the seal contacts the opposing surface.

Another very consequent result can be observed in the seal flow graphs. Increasing the preload pressure drives the seal closer to the opposing surface, making the air gap narrower. The narrower air gap restricts the seal flow more efficiently, and thus the seal flow reduces with the increasing preload pressure. Further, the chamber pressure has little or negligible effect on the seal flow.

Table 2 presents the characteristic values of the system at the highest performance operating point with four different run-outs of the opposing surface. The point of highest performance was defined to be the point where the frictional moment was 1 Nm and the chamber flow was 0 l/min, i.e., where the contours determined previously intersect. The values show that increasing the run-out consequently decreases load capacity and increases the seal flow rate. However, the load capacity met quite closely the theoretical load capacity values, which were calculated using a uniform pressure distribution within the area of the device: the maximum difference 7.7% was detected predictably with the highest run-out of 3.804 mm.

Table 2
The characteristic values of the system at the operating point with highest performance in each measurement. The operating point with highest performance was the point with highest load capacity where friction was 1 Nm and chamber flow was 0 l/min. The theoretical load capacity is calculated assuming that the whole area of the bearing, including the chamber and the seal has a uniform pressure distribution equal to the chamber pressure.

Measurement	Run-out (mm)	Chamber pressure (MPa)	Preload pressure (MPa)	Seal flow (l/min)	Load capacity (kN)	Theoretical load (kN)	Difference (%)
1	0.330	0.46	0.50	8.37	18.86	18.52	1.8
2	1.201	0.42	0.48	9.57	17.24	16.91	1.9
3	2.633	0.36	0.42	10.35	15.13	14.49	4.2
4	3.804	0.28	0.38	11.96	12.22	11.27	7.7

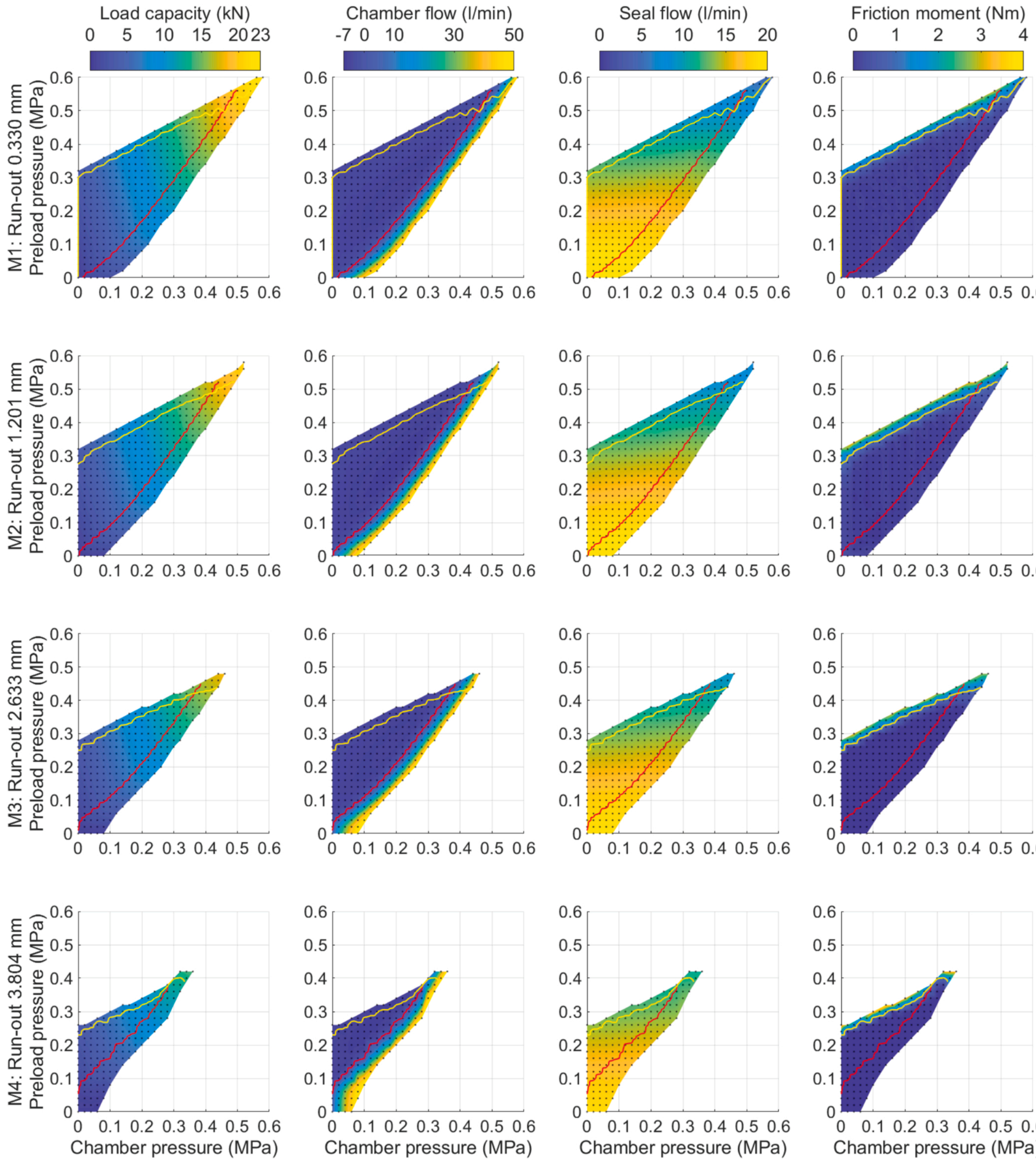

Fig. 9. Measured load capacity, chamber and seal flows, and friction moment of the investigated bearing. Measurement points are shown with black dots. Red contour in the load capacity graph is 0 l/min chamber flow and the yellow contour is 1 Nm friction moment. The rotating speed of the opposing surface was kept constant at 260 rpm.

4. Discussion

4.1. Analysis of the results

The bearing was designed on the basis of flexible seal that can be preloaded against the opposing surface. In order to achieve the desired operation, it is important to lower stiffness in the preload mechanism than the stiffness of the air gap. Therefore, a flexible silicone hose was used as the preload mechanism. In addition, the weight of the seal adversely affects the dynamics of the seal, as it has to follow rapid movement of the opposing surface. Thus, the seal body was manufactured out of aluminium with a minimal cross-section to reduce its inertia.

The results of the present study clearly show that the sealed chamber bearing is functional, can produce high loads close to the theoretical maximum and can be operated under high axial run-out conditions. Consequently, the highest load capacity and broadest operating range was found with the smallest misalignment of the opposing surface. Increasing the misalignment and thus making the conditions more arduous for the bearing, reduced both the load capacity and the operating range. However, the load capacity can be considered more than satisfactory, especially compared to the theoretical maximum loads.

In order to find the suitable operating points and especially the point with the highest performance, limits were placed for the flow rate into the chamber and for the friction moment. The air flow into the chamber, that corresponds to the leakage out of the chamber, was limited to 0 l/min (red contour in Fig. 9). Respectively, the friction moment, that originates from the contact with the opposing surface was limited to 1 Nm (yellow contour in Fig. 9). The operating point with highest load capacity, subjected to these limits, was selected from each measurement at different opposing surface run-out. The red and yellow contours as well as the limits of the measuring range show similar behavior: with the low run-out measurements measurable range and the contours limit fairly smooth triangle-like operating parameter range. When the run-out is increased, the graphs show much higher variation further away from a linear relationship between the chamber and preload pressures. This indicates that the increased run-out, i.e., movement of the opposing surface increased the non-linear behavior of the system.

The chamber flow rate curve of 0 l/min divides the operating points to the two aforementioned operating modes (Fig. 2). The negative chamber flow is due to the seal supply gas flowing into the chamber, and the pressure regulator exhausting gas in order to keep the pressure in the chamber at the set level. In contrast, at the lower edge of the operating parameter map, the seal leakage increases rapidly as the seal gap increases due to the seal preload being insufficient to push the seal against the opposing surface. The chamber design could be potentially realized without a supply to the chamber of the device and pressurizing it only by the seal gas flowing in. With the chamber supply omitted, the bearing could be operated at the operating points of the red contour, after the start-up transient of pressurizing the chamber. This could be used as a simplification in some solutions.

The seal flow decreased as the preload pressure increased; presumably this is based on the flow restriction of the air gap increasing as the air gap decreases. Additionally, the higher pressure in the chamber also limits the flow from the seal supply into the chamber and when the chamber pressure is higher than the pressure in the seal gap, the flow direction reverses. The decreasing seal flow reduces the required compressor power to supply the seal with pressurized air. Therefore, it is advantageous to find a balance between the friction losses and air consumption of the system.

Increasing the run-out of the opposing surface reduces the suitable operating points of the bearing, thus reducing the maximum load capacity. Presumably, the decrease of performance can be attributed to the dynamics of the seal. The inertia of the seal results in the seal lagging behind in phase in relation to the opposing surface, resulting in unsteady air gap height. The unsteady air gap height can lead to periodic contact with the opposing surface and periodic leakage due to increased air gap height. Therefore, it is advantageous to design the seal to be as lightweight as possible in order to maintain the proper air gap height.

The robustness of the bearing against wear was not quantitatively measured during the experiments. Therefore, the wear of the seal was inspected visually (Fig. 10). Some deeper scratches and polished areas appeared on the graphite face of the seal during the measurements (Fig. 10). The damage to the seal is assumed to be caused by the contact between the seal and the opposing surface, which occurred with certain operating parameters, and is indicated by the friction moment measurements in Fig. 9. Presumably, the scratches resulted from dirt or other foreign particles that got caught between the seal and the opposing surface, as the test were conducted in a machine-shop-like environment. The dirt or particles might have been embedded to the face of the seal during its manufacturing process, as during the operation the direction of the air flow is out of the gap, thus purging particles away from the seal gap or the air flow was too weak to stop the particles from entering the gap. However, the wear of the graphite surface of the seal did not seem to affect the performance of the bearing. Additionally, graphite was deposited on the steel disk used as the opposing surface (Fig. 10). The high robustness of graphite restrictor air bearings is well known due to the lubricating properties of graphite, which is further improved by the flexible mounting of the seal limiting the contact forces. The relatively good surface finish of the opposing surface reduces the wear rate of the seal during contact.

The sealed bearing unit that was investigated in the present study has increased load capacity and robustness when compared to current air bearings, both porous or orifice type. However, the increased robustness is at the cost of stiffness. The stiffness of a sealed chamber bearing is much lower than the stiffness of the current bearings. Therefore, the sealed chamber bearing is not a feasible solution to many of the current applications of air bearings where high positional accuracy is required from the bearings. However, the proposed design could be feasible for other applications where use of typical air bearings is limited or infeasible due to tolerance requirements, such as the aforementioned large flexible rotors.

The uncertainty of the measurements was not separately analyzed since it was out of the scope of this study. However, the accuracies announced by the manufacturers of the sensors used in the measurements can be found in Table 1. Taking these accuracy ranges into account, the results of this study remain valid, as the core of the study was not to acquire the most accurate absolute values for the measured

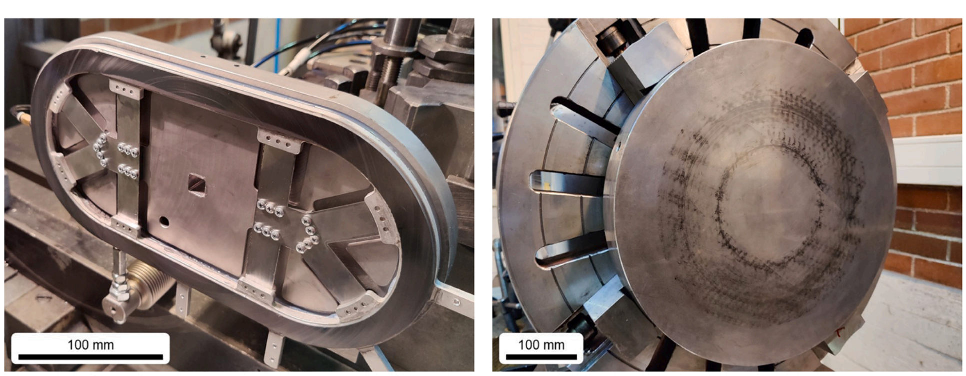

(a) Bearing surface. (b) Opposing surface.

Fig. 10. Wear of the bearing surface (a) and the opposing surface (b). Notice the scratches visible on the graphite seal face. Some of the scratches open a "path" from the pressure chamber to the atmosphere. However, no detectable change in the performance was detected due to the wear marks on the graphite during the course of the measurements. Graphite has been deposited on the steel disk due to a contact with the seal face.

quantities, but to verify the method and to compare the behavior of the device under various conditions.

4.2. Impact

The authors are not aware of earlier published research on a bearing based on an aerostatically sealed pressure chamber, and thus the work can be considered novel. As such aerostatic bearings and seals, including their performance analysis belong to the current body of knowledge. However, the design and intended application of the presented novel bearing differs significantly from the present aerostatic bearings.

One of the main contributions of the study is that the demonstrated bearing required only moderate manufacturing tolerances, due to the flexible mounting of the seals. In addition, despite occasional contact with the opposing surface, the wear of the aerostatic sealing graphite did not affect the performance, despite visually observable wear marks and scratches. The wear resistance of the graphite is of utmost importance in applications where contacts with the opposing surface may occur due to misuse or failures in the air supply, mechanical system or control system. These facts suggest that the robustness of the aerostatic bearing construction method developed in the study is at a high level.

The results of the study enable the further development and investigation of the pressurized chamber based bearing in applications where contactless and frictionless load carrying capacity is needed. Naturally, this kind of applications are of interest in the common strive towards sustainable industry. One very promising application is the deflection compensated rotor (Fig. 1). The performance of the investigated bearing proves the feasibility of using aerostatic bearings instead of hydrostatic or hydrodynamic bearings in applications with flexible rotors. Albeit the in-depth comparison of total energy consumption is outside of the scope of the present study, the authors estimate that the savings due to reduction of friction losses are significant. The present study demonstrates the feasibly of aerostatic bearings that tolerate the appropriate amount of run-out and have enough load capacity to mandate further development.

4.3. Further research

Further research should focus on the dynamic behavior of the bearing, including the effects of damping and high compressibility of the air in the pressure chamber. Investigation of the frequency response of the bearing over a board range is vital for further development of the chamber based bearings. Additionally, the construction and performance of the proposed aerostatic bearing design should be investigated in the case of curved or cylindrical surfaces, the focus being particularly in applications considering rotating machines. Finally, as the load capacity is obviously limited by the bearing area and pressure, increasing the supply pressure beyond typical supply network pressures should be studied. The bearing in the present study was operated at a maximum of 0.6 MPa supply pressure. However, aerostatic graphite seals have been operated at much higher pressure levels. Feasibility of the higher pressure systems should additionally consider the increasing compressor power requirements, which partially cancel out the possible energy savings.

5. Conclusion

The present study developed, realized and experimentally verified a method to construct an air bearing by sealing a pressure chamber with flexibly supported porous aerostatic seals. The results of the study suggest that the method and design are feasible: .

- The realized device had a high load carrying capacity, had a high resilience against misalignment of the opposing surface, wear, and scratches.
- The air consumption of the bearing was reasonable; 8.37 l/min to 11.96 l/min at the highest performance range.
- The load capacity of the bearing was dependent on the run-out of the opposing surface; higher run-out reduced the load capacity. The measured load capacity was 18.86 kN at 0.330 mm run-out, and 12.22 kN at 3.804 mm run-out.
- The suitable operating range of the bearing was limited by the contact friction and leakage from increasing air gap height.

The present study opens new possibilities for air bearing applications, which require higher load carrying capacity that is expected from aerostatic bearings, and robustness against moderate manufacturing tolerances, vibration and wear. In further research, the design and performance of the chamber based aerostatic bearings for cylindrical surfaces of rotor shafts and the rotor dynamic behavior of the system should be investigated. Furthermore, the dynamic stiffness and damping characteristics of the device should be investigated by measuring the frequency response of the device over a broad frequency range.

Declaration of Competing Interest

The authors declare that they have no known competing financial interests or personal relationships that could have appeared to influence the work reported in this paper.

Acknowledgements

This research was funded by the Academy of Finland as a part of the AI-ROT project (grant number 335717). The research was funded also by the 19ENG07 Met4Wind project, which has received funding from the EMPIR programme co-financed by the Participating States and from the European Union's Horizon 2020 research and innovation programme. Additionally, the research was also funded by Aalto University.

References

[1] European Comission, The european green deal, 2020.⟨https://ec.europa.eu/info/sites/info/files/european-green-deal-communication_en.pdf⟩.
[2] Holmberg K, Siilasto R, Laitinen T, Andersson P, Jäsberg A. Global energy consumption due to friction in paper machines. Tribol Int 2013;62:58–77. https://doi.org/10.1016/j.triboint.2013.02.003.
[3] P., Korpelainen, Hydrostaattisen kuormituselementin parametrien vaikutus tehontarpeeseen, Masters thesis, Lappeenrannan teknillinen korkeakoulu, 1999.
[4] Gao Q, Lu L, Chen W, Wang G. Aerostatic bearings design and analysis with the application to precision engineering: state-of-the-art and future perspectives. Tribol Int 2019;135:1–17. https://doi.org/10.1016/j.triboint.2019.02.020.
[5] Fourka M, Bonis M. Comparison between externally pressurized gas thrust bearings with different orifice and porous feeding systems. Wear 1997;210:311–7. https://doi.org/10.1016/S0043-1648(97)00079-3.
[6] K. , Feng , P. , Wang , Y. , Zhang , W. , Hou , W. , Li , J. , Wang , et al. , Novel 3-D printed aerostatic bearings for the improvement of stability: Theoretical predictions and experimental measurements, Tribology International 163, 2021,.10.1016/j.triboint.2021.107149.
[7] D., Ghodsiyeh, F., Colombo, L., Lentini, T., Raparelli, A., Trivella, V., Viktorov, An infinite stiffness aerostatic pad with a diaphragm valve, Tribology International 141 (2020).10.1016/j.triboint.2019.105964.
[8] Theisen LR, Niemann HH, Santos IF, Galeazzi R, Blanke M. Modelling and identification for control of gas bearings. Mech Syst Signal Process 2016;70–71:1150–70. https://doi.org/10.1016/J.YMSSP.2015.09.016. ⟨https://www.sciencedirect.com/science/article/pii/S0888327015004112⟩.
[9] Theisen LR, Niemann HH, Galeazzi R, Santos IF. Enhancing damping of gas bearings using linear parameter-varying control. J Sound Vib 2017;395:48–64. https://doi.org/10.1016/j.jsv.2017.02.021.
[10] Morosi S, Santos IF. Active lubrication applied to radial gas journal bearings. Part 1: modeling. Tribol. Int 2011;44:1949–58. https://doi.org/10.1016/J.TRIBOINT.2011.08.007.
[11] Maamari N, Krebs A, Weikert S, Wegener K. Centrally fed orifice based active aerostatic bearing with quasi-infinite static stiffness and high servo compliance. Tribol. Int 2019;129:297–313. https://doi.org/10.1016/j.triboint.2018.08.024.
[12] Nield DA, Bejan A. Convection in Porous Media. 5.,. New York: Springer International Publishing; 2017. https://doi.org/10.1007/978-3-319-49562-0.
[13] Y., Otsu, M., Miyatake, S., Yoshimoto, Dynamic Characteristics of Aerostatic Porous Journal Bearings With a Surface-Restricted Layer, Journal of Tribology 133 (2011) 11701–1–10.10.1115/1.4002730.

[14] Plante JS, Vogan J, El-Aguizy T, Slocum AH. A design model for circular porous air bearings using the 1D generalized flow method. Precis Eng 2005;29:336–46. https://doi.org/10.1016/j.precisioneng.2004.11.011.
[15] Luong TS, Potze W, Post JB, Van Ostayen RA, Van Beek A. Numerical and experimental analysis of aerostatic thrust bearings with porous restrictors. Tribol Int 2004;37:825–32. https://doi.org/10.1016/j.triboint.2004.05.004.
[16] Messenger A, Williams R, Ingram G, Hogg S, Reggentin P. Demonstration of a dynamic clearance seal in a rotating steam test facility. Proceedings of the ASME Turbo Expo, 8; 2019. p. 1–13. https://doi.org/10.1115/GT2019-91605.
[17] Messenger A, Williams R, Ingram G, Hogg S, Tibos S, Seaton J, et al. Experimental and numerical development of a dynamic clearance seal for steam turbine application. Proceedings of the ASME Turbo Expo, 8; 2016. p. 1–12. https://doi.org/10.1115/GT2016-56995.
[18] Zimmermann AL, Giepman RH, Nguyen Tran QT, Aalburg C, Gümmer V. Design of a static test rig for advanced seals and air bearing testing. Open Archives of the 17th International Symposium on Transport Phenomena and Dynamics of Rotating Machinery, ISROMAC 2017. 2017. p. 1–12.
[19] Zimmermann A-L, Guemmer V, Nguyen T, Giepman RHM. Experimental Investigation and Numerical Validation of the Bearing Face Flow of an Adaptive Seal. Proceedings of the ASME Turbo Expo 2018: Turbomachinery Technical Conference and Exposition, 7B: Structures and Dynamics; 2018. p. 1–9. https://doi.org/10.1115/GT2018-75503.
[20] Wilhelm J, Schwitzke C, Bauer H-J, Nguyen T. A new approach for scaling aspirating face seal aerodynamics. J Eng Gas Turbines Power 2018;141:1–6. https://doi.org/10.1115/1.4041515.
[21] Devitt AJ, Kirkpatrick AD. A precision air bearing stage, containing a moving vacuum chamber. Proc ASPE Spring Top Meet Chall Intersect Precis Eng Vac Technol, ASPE 2006 2006;38:51–3.
[22] Khim G, Park CH. A rotary stage in a vacuum using an air bearing. Vacuum 2014;105:39–45. https://doi.org/10.1016/j.vacuum.2014.01.031.
[23] N., Heidler, Untersuchungen zylindrischer Gasführungselemente für Hochvakuumanwendungen, Ph.D. thesis, Technische Universität Ilmenau, 2015.⟨https://www.db-thueringen.de/receive/dbt_mods_00027178⟩.
[24] International Standard Organisation, ISO 21940–12:2016 Mechanical vibration. Rotor balancing. Part 12: Procedures and tolerances for rotors with flexible behaviour, 2016.
[25] W.H., Rasnick, T.A., Arehart, D.E., Littleton, P.J., Steger, Porous graphite air-bearing components as applied to machine tools, Technical Report, Society of manufacturing engineers, Dearborn, 1974.⟨https://www.osti.gov/servlets/purl/5110726⟩.
[26] M., Hübner, Characterisation of a pressure chamber loading element with aerostatic seals, Master's thesis, Technische Universität Ilmenau, 2021.
[27] J.P., Khatait, W., Lin, W.J., Lin, Design and development of orifice-type aerostatic thrust bearing, Technical Report, SIMTech technical reports, 2005.
[28] International Standard Organisation, ISO 1101:2017 Geometrical product specifications (GPS). Geometrical tolerancing. Tolerances of form, orientation, location and run-out, 2017.

Mikael Miettinen was born in 1995. He has received his M. Sc. degree in mechanical engineering from Aalto University in 2020, where he is currently pursuing a D. Sc. degree in mechanical engineering. In his master's thesis he developed an aerostatically sealed pressure chamber. His current research topics include porous aerostatic bearings and seals with focus on applications with large rotors.

Valtteri Vainio was born in 1995. He has received his M. Sc. degree in mechanical engineering from Aalto University in 2021. Currently, he is pursuing a D. Sc. degree in mechanical engineering at Aalto University. In his master's thesis he investigated the manufacturing and performance measurement of porous material aerostatic bearings. Current research topics include porous aerostatic bearings with focus on manufacturing methods.

René Theska was born in 1957. He received his degrees Dipl.-Ing. (1983) and Dr.-Ing. (1989) in Precision Engineering from TH Ilmenau / TU Ilmenau, Germany. He worked in the industry from 1990 till 2001. Most of this time he worked on tactile and optical CMM technology as the head of R&D at Hexagon Metrology in Wetzlar, Germany. 2001 he was appointed as Professor for Precision Engineering at TU Ilmenau. His research focus is on ultra-precision devices for the measurement of length, force and torque.

Raine Viitala was born in 1992. He received his M. Sc. and D. Sc. degrees in mechanical engineering from Aalto University in 2017 and 2018, and was appointed Assistant Professor in 2020. His doctoral dissertation was acknowledged with the Aalto University School of Engineering dissertation award. In 2018, Viitala visited Technische Universität Darmstadt researching rotating kinetic energy storages, i.e., flywheels. Viitala has a solid background in experimental large rotor research, including vibration analysis, bearing excitations, roundness measurements and manufacturing for operating conditions. His work is widely applied in several industrial applications, such as electric motors and generators, turbines, and paper machines. He is instructing students at all academic levels, and is the responsible teacher of Mechatronics minor at Aalto University.